8-2011

Positional Control Over Nanoparticle Deposition into Nanoholes

Moshood K. Morakinyo
Portland State University

Shankar B. Rananavare
Portland State University, ranavas@pdx.edu

Positional Control Over Nanoparticle Deposition into Nanoholes

Moshood K. Morakinyo and Shankar B. Rananavare

***Abstract*— Controlled deposition of metal nanoparticles (NPs) into lithographic patterned nanoholes has been a major challenge. Electrostatic attraction was employed in directing gold NPs of precise size into e-beam lithographically patterned holes. Citrate stabilized gold NPs with a net negative surface charge were deposited on a positively charged well-bottom surface generated by adsorption of long-chain amino-terminated organosilane N-(2-aminoethyl)-11-aminoundecyltrimethoxy- silane (AATMS). Scanning electron microscopy (SEM) results indicate that deposition of NPs into patterned holes is a function of deposition time and NPs concentration. Other factors affecting NP fill fraction are thickness of silane and resist layer and spacing between the nanoholes.**

Index Terms - Gold nanoparticles, nanoholes, N-(2-aminoethyl)-11-aminoundecyltrimethoxy- silane, electrostatics

I. Introduction

THE interest in gold nanoparticles (Au NPs) for nanoscience and nanotechnology applications has grown significantly in recent years due to their unique electronic, magnetic, optical and catalytic properties [1;2]. Au NPs are highly resistant to oxidation at temperatures below its melting point [3]. Apart from being one of the most stable metal NPs, Au NPs of precise nano-sizes can be conveniently and reproducibly synthesized [4-8]. These properties make Au NPs to be super star NPs suitable for the engineering of nanoscale devices and for nano-medicine, especially when compared with other coinage metals (silver and copper) [9]. Placement of these gold NPs on the desired location as well as their organization into controlled architectures is very crucial for their various applications. Such placement and organization could be used as templates for pattern transfer in SiO_2 substrates by reactive ion etching (RIE). Several placement techniques have been proposed including physical, molecular and electrostatic templates [10;11]. Koh's group has demonstrated placement of one gold nanoparticle per hole by electrostatic funneling technique, involving creation of negatively charged environment around positively charged e-beam patterned holes[12]. Negatively charged gold NPs were guided into holes by a combination of repulsive and attractive forces.

In this study, we report the effectiveness of electrostatic interaction between negatively charged surfaces of Au NPs and positively charged amino end of N-(2-aminoethyl)-11-aminoundecyltrimethoxy- silane (AATMS). A long chain aminosilane, AATMS, was used due to its special hydrolytic stability and its ability to form stable self assembly for gold NPs deposition. Asenath-Smith and Chen have shown that aminosilanes with longer alkyl linker than propyl are stable in aqueous solutions [13]. Also, unlike short chain 3-aminoprpyltriethoxysilane (APTES), the most widely used molecule for surface silanization AATMS can undergoes island-type growth that produces uniform films [14]. Present studies describe a characterization and development of deposition protocol. It includes characterization of self-assembled mono/multilayers (SAMs) using contact angle, and XPS methods. Factors affecting gold NP deposition are presented. Fig. 1 is a flow chart of our strategy for electrostatic deposition of Au NPs (citrate stabilized with a negatively charged surface) into e-beam lithographically patterned nanoholes. This initial study does not employ negatively charged resist layer (i.e., electrostatic funnelling). After gold deposition, the resist can be removed leaving a well-organized array of immobilized gold NPs which can be used to produce a variety of nanoelectronics and sensor components. Our long term objective of this study is to position particles not only in nanoholes but in nanotrenches as well as pattern transfer in SiO_2.

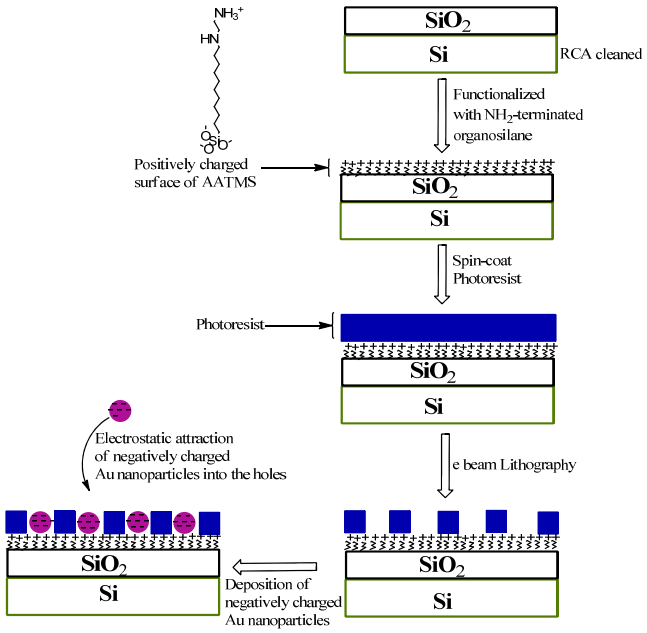

Fig. 1 Schematic representation of the strategy for electrostatic deposition of gold NPs into e-beam lithographically patterned nanoholes. (Layer thicknesses are drawn for illustration only.)

Manuscript received June 15th,2011. This work was supported by the Intel Corp. and Oregon Nanotechnology and Microtechnology Initiative (ONAMI).

Moshood K. Morakinyo is with the Portland State University, Portland OR 97207, mmorkin@pdx.edu.

Shankar B. Rananavare is with the Portland State University, Portland OR 97207, Phone:503-725-8511, Fax: 503 725 9525, email: ranavas@pdx.edu.

II. EXPERIMENTAL METHODS

Materials: The following chemicals were used without further purification: Gold colloids (Ted Pella Inc.); hydrogen peroxide, hydrochloric acid, ammonium hydroxide (Fisher Scientific); toluene (anhydrous, 99.8 %), (3-aminopropyl) triethoxysilane (APTES, 99 %,), poly(methyl methacylate (PMMA, 5 %) (Sigma-Aldrich); N-(2-aminoethyl)-11-aminoundecyltrimethoxysilane (AATMS, >95 %, Gelest Inc.). Doubly-distilled and deionized water (Barnstead Sybron Corporation water purification Unit, resistivity of 19.0 MΩcm) was used for cleaning apparatus and for washing substrates.

Derivatization and characterization: The surface of silicon wafers were pre-cleaned prior to derivatization with aminosilanes (APTES or AATMS) by modified RCA clean method (SC1: H_2O_2:NH_4OH:H_2O = 1:1:5 v/v and SC2: H_2O_2:HCl:H_2O = 1:1:5 v/v) to maximize the number of silanol group on the surface [15;16]. Samples were incubated in 0.05 M solution of AATMS or APTES, prepared in dry toluene at 80 °C for 20 minutes, sonicated in pure toluene for 5 minutes and then dried in a stream of nitrogen gas. Surface characterization was done by a number of complementary techniques. Contact angle measurements were conducted using Kodak MDS100 camera and the corresponding images were analyzed using a contact angle macro in Image-J software freely available from NIH website. Film thickness measurement used a Gaertner ellipsometer (He-Ne laser light source, λ = 632.8 nm, fixed incidence angle of 70 °C). Surface elemental compositions were characterized by x-ray photoelectron spectroscopy (XPS, ThermoScientifc ESCALAB 250 instrument).

E-beam patterning: Aminosilane derivatized wafer coated with PMMA resist was patterned using e-beam (Zeiss sigma VP FEG SEM) to produce nanoholes.

Gold NP deposition: Two methods were employed for the deposition of Au NPs. First method involves immersion of pre-patterned wafers in Au NP solutions. Deposition was achieved in 24 to 48 hours depending on NP sizes and hole diameters. Second method was by evaporation-induce deposition of Au NPs. This was done by spraying Au NPs solution onto the patterned substrates followed by controlled evaporation at temperatures slightly above room temperature. Excellent deposition was obtained within 10 minutes. After deposition samples were washed with deionized water and then dried in a stream of nitrogen gas.

Scanning electron microscopy imaging: An FEI Siron XL30 model SEM was used for electron microscopy imaging. Imaging was performed at an accelerating voltage of 5 kV at beam current of ~300 μA.

III. RESULTS AND DISCUSSION

Organosilane derivatized surface was characterized by ellipsometry, water contact angle measurements (Table 1) and XPS (Table 2). The thickness of native SiO_2 layer that was produced after RCA clean was determined to be 1.4 ± 0.3 nm. This thickness of SiO_2 was in good agreement with literature value of 1.6 ± 0.1 nm obtained by Pasternack and co-workers after RCA clean [17]. Data in Table 1 clearly show that organosilane (AATMS) film thickness increased with increase in derivatization time.

Table 1: Contact angles and film thicknesses of AATMS on SiO_2 surface before and after silanization.

Silanization time of AATMS (minutes)	AATMS film thickness by ellipsometry (nm)	Water contact angle
0.0 (before silanization)	0.0	0
10.0	2.9 ± 0.4	52 ± 4°
20.0	9.0 ± 0.2	54 ± 3°
30.0	14.4 ± 0.2	54 ± 4°
40.0	16.5 ± 0.2	51 ± 4°
50.0	19.5 ± 0.3	51 ± 3°
60.0	22.0 ± 0.5	59 ± 3°

A plot of AATMS film thickness versus derivatization time showed zero-order dependence with an intercept kinetically indistinguishable from zero (Fig.2).

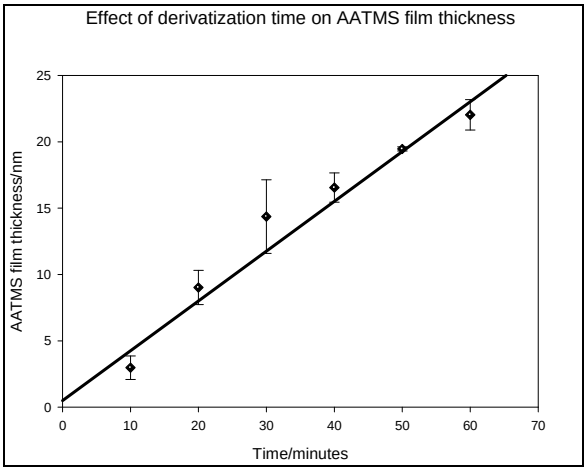

Fig. 2 A plot showing the effect of derivatization time on AATMS film thickness. The plot shows a zero order dependence in derivatization time with intercept kinetically indistinguishable from zero.

Despite a progressive increase in AATMS film thickness with derivatization time, water contact angles (55±5°) were relatively constant. This range of water contact angles for AATMS agreed with previously obtained values for amino-terminated organosilanes [13] suggesting a thickness independent surface polarity.

Table 2 shows detected binding energies and atomic percentages for different functionalities on the surfaces of AATMS derivatized and non-derivatized substrates measured by XPS. Of particular importance were the increase in atomic percent of total hydrocarbon from 7 % on the non-derivatized surfaces to 42 % on the AATMS derivatized surfaces; and the appearance of N-containing functionalities (C1s C-N at 286.0 eV, N1s C-N at 400.1 eV and N1s NH_3^+ at 401.4 eV) on the derivatized surfaces. The increase in hydrocarbon concentration could be attributed to hydrocarbon portion of the organosilane. Also the N-containing functionalities were consistent with amino end-groups of AATMS. These XPS results confirmed derivatization of silicon substrates.

Table 2: XPS analysis of blanket non-functionalized silicon wafer and AATMS functionalized wafer.

Functionality	Non-functionalized wafer		AATMS functionalized wafer	
	Binding energy (eV)	At %	Binding energy (eV)	At %
Hydrocarbon	284.8	7	284.8	42
C1s C-O	286.2	2	286.4	7
C1s C=O	287.1	1	287.5	2
C1s O-C=O	288.8	1	288.3	2
C1s C-N	**-**	**0**	**286.0**	**5**
N1s C-N	**-**	**0**	**400.1**	**4**
N1s NH_3^+	**-**	**0**	**401.4**	**2**
O1s	532.4	27	532.4	11
O1s	-	-	531.7	4
Si2p	98.7	54	98.3	11
Si2p, SiO_x	102.6	9	102.3	7

Gold NP deposition on APTES and AATMS: Gold deposition was carried out on APTES and AATMS derivatized surfaces. As shown in Figs. 3a and b, AATMS derivatized surface produced a denser film of Au NP (particle density of 650 particles/μm^2) than APTES derivatized surface (particle density of 406 particles/μm^2) for depositions carried out under the identical conditions; 12 hours of deposition at room temperature. This could be a reflection of island-type of film growth usually obtained in long chain organosilanes which is absent in short chain organosilanes like APTES [14]. Island-type of growth leads to continuous, denser films, which are expected to favor higher deposition density for Au NP, as we observed.

Gold deposition by substrate immersion in gold colloidal solution (Fig. 3c) was compared with gold deposition by evaporation-induced method (Fig. 3d). Within 10 minutes a huge deposition was achieved by evaporation-induced method (particle density of 413 particles/μm^2) which was 122 % more than the deposition density obtained by immersion method (particle density of 186 particles/μm^2).

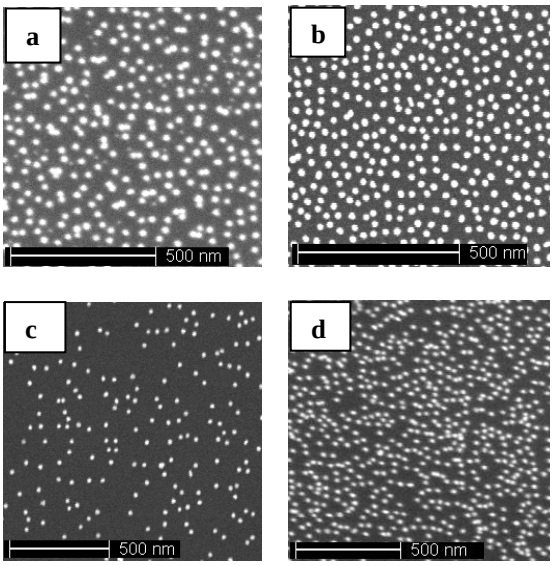

Fig. 3 Deposition of 20 nm Au NPs on (a) 2 % (v/v in toluene) (0.084 M) APTES functionalized wafer; particle density = 406 particles/μm^2 and (b) 2 % (v/v in toluene) (0.053 M) AATMS functionalized wafer; particle density = 650 particles/μm^2. Deposition time = 24 hours. Under the same deposition conditions AATMS produced better gold deposition than APTES. (c) and (d) show 10 minutes 20 nm Au NPs deposition on AATMS substrate by (c) immersion of substrates in Au NP solutions; particle density = 186 particles/μm^2 and (d) evaporation-induced method; particle density = 413 particles/μm^2.

Effect of e-beam on gold deposition on APTES surfaces:
E-beam (30kV) exposure of surface derivatized wafers prior to deposition affected their Au NP binding properties As shown in Fig. 4 particle density of 60 nm Au NPs decreased from 94(unexposed) particles/μm^2, to 46(exposed) particles/μm^2, about ~50 % decrease at a dosage commonly used for e-beam patterning. A significant cleavage of the near surface amine groups by high energy electrons would account for this phenomenon.

Gold NP deposition on patterned substrates: Figs. 5a, b and c show SEM images of 20 nm and 40 nm NPs deposited into e-beam patterned 200 nm holes. Au NPs were guided into the holes by the electrostatic attractive forces between positively charged amino end group (NH_3^+) residing at the bottom of holes and the citrate capped negatively charged Au NPs surface. Within 24 hours only 20 nm size Au NPs were deposited into the holes (Fig. 5a). Significant deposition of 40 nm gold NPs occurred only after 48 hours

(Figs. 5b and c) of deposition period. The concentration of 20 nm Au NPs in the depositing solution was significantly higher than the 40nm Au NPs (8 fold). This implies that the rate of deposition was highly dependent

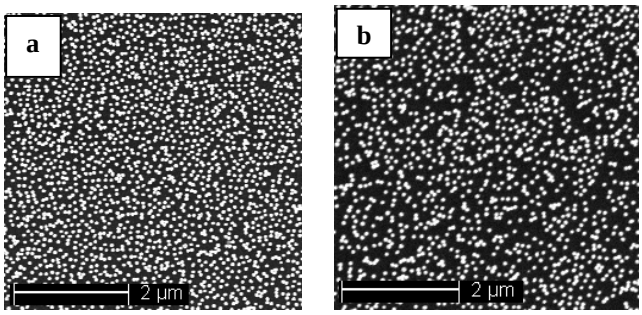

Fig. 4 Effect of e-beam on Au NP deposition. (a) 60 nm Au NPs deposited on APTES derivatized surface before exposure to 30 kV e-beams (particle density of 94 particles/µm^2). (b) 60 nm Au NPs deposited on APTES surface after exposure to 30 kV e-beams (particle density; 46 particles/µm^2).

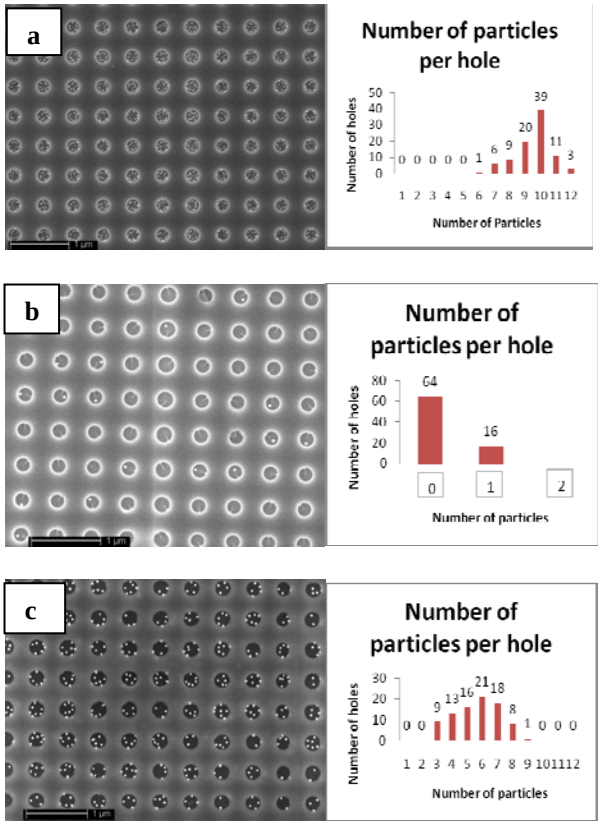

Fig. 5 (a) SEM image of 20 nm gold NPs in the holes after 24 hours of electrostatic deposition. Average number of gold NPs per hole is 9 NPs. (b) SEM image of 40 nm gold NPs in the holes after 24 hours of electrostatic deposition. Here we have one NP per hole but with more empty holes (80.00 %) than holes with NPs (20.00 %). (c) SEM image of 40 nm gold NPs in the holes after 48 hours of electrostatic deposition. Average number of gold NPs per hole is 6 NPs.

on the concentration of Au NPs. Apart from concentrations of Au NPs, other factors that were found to affect deposition were nanohole diameter, pitch and resist/AATMS film thicknesses. As shown in Table 3, Au NPs fill fractions (defined here as a ratio of number of holes with at least one particle to the total number of holes) increased from 0.5 for 80 nm holes to 0.97 for 100 nm holes for 24 hours deposition of 20 nm Au NPs. Similar trend was observed for resist thickness. For example, for 40 nm Au NPs deposition into 200 nm patterned holes fill fractions increase from 0.29 to 0.81 for resist thickness of 64 nm and 185 nm respectively. These results showed that thicker resist films were good for NP deposition into patterned nanoholes. Thicker resist films may promote trapping of NPs in the hole and thus favoring the electrostatic interactions between the derivatized bottom surface of holes and the NPs. Thicker resist films could also reduce the e-beam damage of the positively charged aminosilane surfaces (see above). The same rationale may apply for AATMS thickness dependence on Au fill fraction.

Table 3: Analysis gold NPs deposition over 24 hours into e-beam patterned holes.

NP Diam-eter (d) (nm)	Hole Diam-eter (D) (nm)	PMMA Resist Thickn-ess (S) (nm)	Hole Area Fract-ion (A)	AATMS Film Thickness (s) (nm)	NP fill fractio n (P)
20	80	64	0.020	6.4	0.5
20	100	185	0.031	6.4	0.97
20	220	64	0.152	9.3	1.00
20	80	64	0.196	2.6	0083.
20	80	64	0.196	2.6	0.88*
40	200	64	0.126	9.3	0.29
40	200	185	0.126	9.3	0.81
40	200	185	0.126	9.3	1.00
60	200	64	0.126	9.3	0.027
60	200	185	0.126	9.3	0.20
100	200	185	0.126	6.4	0.067

These studies employed 24 hours of deposition time, with an exception marked with an asterisk (48 hr. deposition time).

Fill fraction was empirically related to the pattern features as follows:

$$P = \frac{C.D.s.S.A}{d}$$

Where C is the NP concentration and other symbols are defined in Table 3. Here for simplicity only direct and inverse relations were assumed. In general these parameters would be expected to have significant nonlinear dependences.

In all the NP depositions studies on patterned holes there was little/no deposition on the unexposed resist film. Most

NPs were inserted inside the holes. The NPs still maintained a relatively the same mean separation observed in the deposition on the blanket (unpatterned) wafers. For example, we found that the mean separation between 20 nm Au NPs to be 10.1 ± 2.0 nm on blanket wafer and 12.0 ± 1.5 nm in patterned holes. This indicated that hole walls were not affecting the interparticle interactions during immersion deposition. But see below.

In order to increase the fill factor to one NP per hole as observed in Fig. 5b there is a need to squeeze the size of holes in comparison with the size of the NPs and then increase the deposition time. Fill fraction of one NP per hole could also be achieved by negatively polarizing the resist film surface near nanoholes by oxygen plasma or ozone treatment, the so called electrostatic funneling[12]. Such studies are currently underway.

Evaporation driven gold NP deposition on patterned substrates: The main problem in the immersion deposition strategy was that it took well over 24 hours to get significant deposition in nanoholes. Therefore, in accordance with equation 1, we explored an evaporation-driven deposition of NPs on patterned substrates as a means of improving the slow kinetics. During solvent evaporation, the increased concentration of NPs should result in faster deposition of NPs. The process was however more challenging to optimize as many parameters had to be precisely controlled. For example, the evaporation had to be done at temperatures well below the glass transition temperature of the resist used for patterning; otherwise the resist would begin to reflow [18]. Fig. 6 shows results of evaporation induced deposition of 50 nm Au NPs into 100 nm patterned holes at 30 °C in ten minutes. The holes were completely filled by aggregates of Au NPs. The deposition pattern is significantly different than the results seen in the immersion deposition (Fig. 5c). Particles preferred to aggregate on the resist sidewalls of nanoholes.

One potential mechanism for such deposition is the influence of progressive reduction in the Debye screening length due to increased solute concentration during evaporation. This shorter range repulsion would permit aggregation. This effect would not be present during the immersion deposition where the ionic strength is low and does not change during deposition. This leads to longer range electrostatic repulsion keeping the NPs well separated from each other.

A second mechanism we considered for this wall deposition is based on removal of solvent As the solvent evaporates from the nanowells, the trapped NPs are forced closer; see Fig 7. During the process, the so called depletion force becomes relevant [19]. The depletion force is always attractive and relevant on sub-nanometer length-scale. Furthermore, the depletion force between the wall and NPs is considerably higher (2-3X) than the corresponding inter-NP depletion interaction. This mechanism also explains why aggregates of Au NPs were not observed during deposition by immersion (Fig. 5a, b and c). In this case, the mean inter-NPs distance remains constant and larger than the length-scale relevant for the depletion interaction throughout the immersion deposition period.

Another salient feature of the deposition pattern is that the Au NPs appear to sink into the resist walls. More studies are needed to verify the topology of deposits and the effect of evaporation temperature, ionic strength, and humidity during this evaporative deposition. Such studies are currently underway.

.

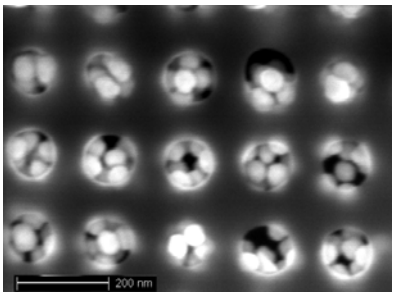

Fig. 6 SEM image of 40 nm gold NPs in the holes by evaporation-induced deposition method. Holes are fully filled with Au NPs. No deposition on the resist.

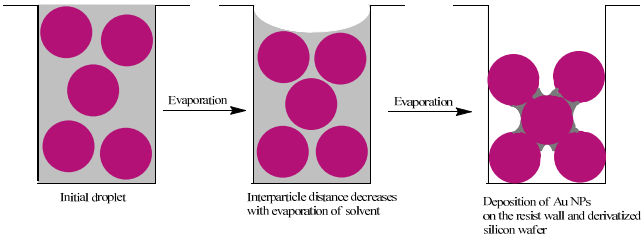

Fig. 7. Schematic illustration of drying induced deposition of Au NPs on the resist walls and derivatized silicon wafer.

IV. CONCLUSIONS

This study focused on targeted gold nanoparticles deposition by electrostatic attraction on blanket and patterned wafers by immersion and evaporative deposition methods. The rate of NP deposition was directly proportional to concentration of NPs in depositing colloidal solution. Significant deposition was achieved within 10 minutes by evaporation method thus overcoming one of the main limitations of the immersion deposition method that typically required at least 24 hours of deposition time. During the immersion deposition, the fill fraction of nanoparticles in an assembly of nanoholes, depended on the thickness of resist and SAM layers, and the ratio of nanohole to particle diameters. During the evaporative deposition, particles preferentially deposited on resist wall, which was rationalized in terms of depletion forces between nanoparticles and the hole wall.

V. ACKNOWLEDGMENTS

This work was supported by Intel corporation grant number 414305 and Oregon Nanotechnology and Microtechnology Initiative (ONAMI). Many simulating discussion with Intel colleague Dr James Blackwell are gratefully acknowledged. We thank Stephen Golledge and Kurt Langworthy at University of Oregon, Eugene, OR, for their help with XPS characterization and e-beam lithography respectively.

VI. REFERENCES

[1] M. C. Daniel and D. Astruc, "Gold nanoparticles: Assembly, supramolecular chemistry, quantum-size-related properties, and applications toward biology, catalysis, and nanotechnology," *Chemical Reviews*, vol. 104, no. 1, pp. 293-346, Jan.2004.

[2] A. N. Shipway, E. Katz, and I. Willner, "Nanoparticle arrays on surfaces for electronic, optical, and sensor applications," *Chemphyschem*, vol. 1, no. 1, pp. 18-52, Aug.2000.

[3] J. C. Love, L. A. Estroff, J. K. Kriebel, R. G. Nuzzo, and G. M. Whitesides, "Self-assembled monolayers of thiolates on metals as a form of nanotechnology," *Chemical Reviews*, vol. 105, no. 4, pp. 1103-1169, Apr.2005.

[4] E. Boisselier, A. K. Diallo, L. Salmon, J. Ruiz, and D. Astruc, "Gold nanoparticles synthesis and stabilization via new "clicked" polyethyleneglycol dendrimers," *Chemical Communications*, no. 39, pp. 4819-4821, 2008.

[5] L. Polavarapu and Q. H. Xu, "A simple method for large scale synthesis of highly monodisperse gold nanoparticles at room temperature and their electron relaxation properties," *Nanotechnology*, vol. 20, no. 18 May2009.

[6] L. Polavarapu and Q. H. Xu, "A single-step synthesis of gold nanochains using an amino acid as a capping agent and characterization of their optical properties," *Nanotechnology*, vol. 19, no. 7 Feb.2008.

[7] O. Fabian, "Synthetic routes to monodisperse gold nanoparticle stabilized by different-length alkanethiols," Massachusetts: Massachusetts Institute of Technology libraries, 2008, pp. 5-30.

[8] H. C. Dong, M. Z. Zhu, J. A. Yoon, H. F. Gao, R. C. Jin, and K. Matyjaszewski, "One-pot synthesis of robust core/shell gold nanoparticles," *Journal of the American Chemical Society*, vol. 130, no. 39, p. 12852-+, Oct.2008.

[9] E. Boisselier and D. Astruc, "Gold nanoparticles in nanomedicine: preparations, imaging, diagnostics, therapies and toxicity," *Chemical Society Reviews*, vol. 38, no. 6, pp. 1759-1782, 2009.

[10] S. J. Koh, "Strategies for controlled placement of nanoscale building blocks," *Nanoscale Research Letters*, vol. 2, no. 11, pp. 519-545, Nov.2007.

[11] S. J. Koh, "Controlled placement of nanoscale building blocks: Toward large-scale fabrication of nanoscale devices," *Jom*, vol. 59, no. 3, pp. 22-28, Mar.2007.

[12] L. C. Ma, R. Subramanian, H. W. Huang, V. Ray, C. U. Kim, and S. J. Koh, "Electrostatic funneling for precise nanoparticle placement: A route to wafer-scale integration," *Nano Letters*, vol. 7, no. 2, pp. 439-445, Feb.2007.

[13] E. Asenath-Smith and W. Chen, "How To Prevent the Loss of Surface Functionality Derived from Aminosilanes," *Langmuir*, vol. 24, no. 21, pp. 12405-12409, Nov.2008.

[14] S. Onclin, B. J. Ravoo, and D. N. Reinhoudt, "Engineering silicon oxide surfaces using self-assembled monolayers," *Angewandte Chemie-International Edition*, vol. 44, no. 39, pp. 6282-6304, 2005.

[15] [Anon], "Study Finds Rca Clean Still the Best Solution," *Solid State Technology*, vol. 38, no. 6, pp. 36-38, June1995.

[16] W. Kern and D. A. Puotinen, "Cleaning Solutions Based on Hydrogen Peroxide for Use in Silicon Semiconductor Technology," *Rca Review*, vol. 31, no. 2, p. 187-&, 1970.

[17] R. M. Pasternack, S. R. Amy, and Y. J. Chabal, "Attachment of 3-(Aminopropyl)triethoxysilane on Silicon Oxide Surfaces: Dependence on Solution Temperature," *Langmuir*, vol. 24, no. 22, pp. 12963-12971, Nov.2008.

[18] S. K. Kim, "Resist reflow process simulation study for contact hole pattern," *Journal of Vacuum Science & Technology B*, vol. 24, no. 1, pp. 200-204, Jan.2006.

[19] J. Goodwin, Colloids and Interfaces with Surfactants and Polymers (Wiley, Chichester, 2004).